Materials & Design 253 (2025) 113822

Contents lists available at ScienceDirect

Materials & Design

journal homepage: www.elsevier.com/locate/matdes

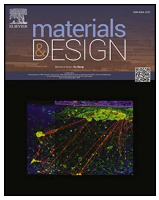

Efficient design of Voronoi energy-absorbing foams using Bayesian optimization

Youngtaek Oh [a], Byungjo Kim [b], Hayoung Chung [a,*]

[a] Department of Mechanical Engineering, Ulsan National Institute of Science and Technology, 50 UNIST-gil, Ulju-gun, Ulsan 44919, Republic of Korea
[b] Graduate School of Semiconductor Materials and Devices Engineering, Ulsan National Institute of Science and Technology, 50 UNIST-gil, Ulju-gun, Ulsan 44919, Republic of Korea

ARTICLE INFO

Keywords:
Lightweight structure
Energy absorption
Voronoi tessellation
Aleatory uncertainty
Kriging
Bayesian optimization

ABSTRACT

Recently, many studies have increasingly focused on developing bio-inspired structures, leveraging their lightweight and high-energy absorption properties, which are crucial across many engineering fields. Structural optimization aiming for bio-inspired structures having superior energy absorption capability, however, has been considered a challenging problem. One of these challenges is that nonlinear material behaviors induced by external forces, such as buckling and self-contact of constituting ligaments, intervene in the energy absorption process. Such nonlinearities not only make the relationship between design changes and energy absorption nonlinear, but also exacerbate the difficulties of design, given the complexity of the ligament configurations. To address this, a novel design optimization method for bio-inspired cellular structures with high energy absorption is proposed. First, Voronoi tessellation is used to capture configurations of bio-inspired material, parameterized by geometric variables. Then, Bayesian optimization with Kriging efficiently updates the design, exploring the complex design space through high-fidelity nonlinear finite element analysis. The proposed design method is efficient in structural optimization as it combines a strategy to reduce the number of samples required for surrogate modeling of structural response and optimal search, but it also generates multiple design outcomes with similar advantages due to the intrinsic variance of the Voronoi structures.

1. Introduction

Over the past few decades, the remarkable mechanical properties of nature-inspired materials—which are engineered to emulate the structural and functional properties of biological materials that have evolved over millions of years—have attracted significant attention in fields such as aerospace, automotive, and defense. These materials exhibit exceptional mechanical characteristics, such as high impact resistance [1,2], superior load-bearing capabilities, and enhanced strength and energy absorption (EA) [3,4,5], which have led to extensive research exploring their potential for real-world applications. For instance, models have been developed to optimize energy absorbers while simultaneously considering both the EA capability of structures and pedestrian safety, with potential applications in automotive bumpers [6]. Additionally, studies have explored the development of bio-inspired functionally graded metamaterials, which exhibit characteristics suitable for use as cushioning materials to mitigate impact forces in the landing legs of space landers [7], as well as nature-inspired functionally graded lattice materials for bridge pier protection, improving crashworthiness against ship collisions [8]. Furthermore, nature-inspired materials have been explored for various biomedical and consumer applications, including scaffolds for tissue engineering [9] and midsoles for footwear [10]. These findings underscore the promise of nature-inspired materials in the development of resilient and high-performance structures across various industries.

Voronoi tessellation has been suggested to project the complex configuration of nature-inspired materials into tractable mathematical descriptions. It is a numerical method that generates non-overlapping convex polygons or polyhedra within the design domain. Voronoi tessellation has been widely utilized in structural design optimization, particularly in non-gradient-based methods, as it enables a wide and diverse search space with a reduced number of design parameters. One of its key advantages is that the patterns obtained through Voronoi tessellation closely resemble those found in nature, enabling the straightforward replication of foam-like structures such as abalone shells [11], porcupine quills [12], and pomegranate shells [13], all of which

* Corresponding author.
E-mail address: hychung@unist.ac.kr (H. Chung).

https://doi.org/10.1016/j.matdes.2025.113822
Received 30 October 2024; Received in revised form 4 March 2025; Accepted 7 March 2025
Available online 12 March 2025

exhibit exceptional EA, efficient energy dissipation, and high impact resistance. Beyond replicating natural patterns, Voronoi tessellation enables fully automated structural design with minimal user intervention, enhancing computational efficiency, particularly in applications involving repeated EA evaluations.

Previous studies have leveraged these benefits to design and analyze Voronoi-based energy-absorbing structures. Ghazlan et al. [11] studied the structure of red abalone nacres and successfully reproduced their complex topology, leading to improved EA capability. More recently, Tee et al. [12] and Ortiz et al. [13] reproduced the intricate patterns of porcupine quills and pomelo peels using Voronoi tessellation and investigated the correlation between Voronoi parameters and the EA capability of the structures.

Thanks to the mathematical tractability of their geometric representation, the geometric characteristics of Voronoi structures—such as their regularity and constituting cell sizes—have been extensively studied in relation to their high EA efficiency. For example, Song et al. [14] conducted a parametric study to enhance the EA ability of Voronoi structures under dynamic crushing conditions. Abdullahi et al. [15] employed particle swarm optimization to determine the optimal Voronoi parameters for multi-cell square tubal structures in a multi-objective optimization framework. In another study, Tung et al. [16] optimized Voronoi parameters for improved EA capabilities using genetic algorithms, incorporating a variety of Voronoi structure images in their analysis. Despite these extensive parametric studies, designing the optimal configurations of Voronoi structures remains a challenging task. Firstly, the design parameters that define Voronoi diagram configurations are only implicitly correlated with mechanical behaviors. For example, while the number of seeds in the Voronoi diagram affects the size of the cells, it does not determine an exact geometric configuration or a deterministic mechanical property. However, this correlation is not entirely random; an increased number of polygons within the domain generally enhances the structure's load-carrying capacity due to the greater number of load paths. Therefore, the design process should be considered a stochastic process with aleatoric uncertainty, where the analytical derivation of design sensitivity—essential for utilizing gradient-based optimization—is not feasible. Furthermore, the complexity is exacerbated by the intricate EA behaviors involved in mechanically loaded Voronoi structures, including extensive contact and ligament buckling, which are both unknown a priori and computationally expensive.

While numerous studies have explored designs of Voronoi structures, the aleatory uncertainties in Voronoi parameters, which determine the shape and number of polygons within the structure, are largely not taken into account. Instead, designs have often been developed by manually selecting specific configurations of Voronoi structures within the design space, then either choosing the best sample from the selection or using those samples for further refinement [17]. While this approach simplifies the design process, it inadvertently restricts the full exploration of the design space and limits the potential performance of Voronoi structures. Furthermore, even when uncertainty is considered, handling randomness typically relies on averaging multiple objective function evaluations with respect to a design variable, resulting in significant computational costs [15]. These two key limitations—restricted design space exploration and high computational cost—highlight the need for a more systematic and efficient design framework for Voronoi structures.

Given the black-box relationship between Voronoi parameters and the EA performance of Voronoi structures, as well as the inherent randomness of the structures, Bayesian Optimization (BO)—an efficient non-gradient optimization method for handling highly nonlinear analyses— offers a powerful solution. Bayesian optimization excels at managing black-box functions [18,19], which is crucial given the unclear relationship between Voronoi structures and their EA capabilities. Furthermore, by utilizing probabilistic surrogate models, BO effectively incorporates aleatory uncertainty from random design variables into the surrogate model, making it particularly effective for optimizing highly nonlinear functions and handling noisy variables more efficiently than other non-gradient-based optimization methods. Owing to these advantages, the adoption of BO in structural design has steadily increased. For instance, Shin et al. [20] applied BO to optimize spiderweb nanomechanical resonators, successfully managing complex variable interactions while minimizing computational costs. Likewise, Kaczmarski et al. [21] addressed the control challenges posed by the infinite degrees of freedom in soft actuators using BO on reduced-order models, providing a robust and efficient design and control strategy. Park et al. [22] employed BO to optimize staggered platelet composite structures, managing the intricate relationship between structural configuration and toughness. By incorporating experimental toughness data and accounting for aleatory uncertainty arising from inconsistent experimental conditions, they effectively integrated the intrinsic variance into the probabilistic surrogate model. Despite these successful applications in structural designs, the use of BO for optimizing Voronoi structures remains unexplored, highlighting the need for a comprehensive framework to fully leverage its potential.

In this study, a novel design framework is introduced to overcome the limitations of previous Voronoi-based structural designs, specifically restricted design space exploration and high computational cost. The proposed framework accounts for the aleatory uncertainty of Voronoi parameters without limiting the design space, enabling a more comprehensive exploration while significantly reducing computational cost. By employing Kriging as a probabilistic regression model, the framework captures the nonlinear relationship between Voronoi structures and EA capability under uniaxial compression, integrating EA variance into the correlation matrix to account for the inherent randomness of Voronoi parameters. This approach not only broadens design space exploration but also reduces reliance on manual design, facilitating the generation of multiple high-performing Voronoi configurations with minimal human intervention. Furthermore, by efficiently identifying the optimal Voronoi parameters with fewer function evaluations, the framework enables the generation of additional configurations with superior mechanical properties, all derived from the optimal Voronoi parameter. By addressing these fundamental challenges, this study establishes a methodology for Voronoi-based structural optimization, expanding its applicability across various engineering domains.

The remainder of this paper is organized as follows: Section 2 introduces the method for parameterizing the design domain using Voronoi tessellation and describes the FE analysis of Voronoi structures to evaluate their EA capabilities. Section 3 outlines the problem statement for structural optimization aimed at maximizing the EA of Voronoi structures and provides a theoretical foundation of the proposed design framework. Section 4 presents the optimization results using the proposed framework, validates its effectiveness and accuracy through comparative studies, and investigates the influence of Voronoi design parameters on EA performance. Finally, Section 5 concludes the paper with key findings and offers insights into future research directions.

2. Modeling of Voronoi structures

2.1. Voronoi tessellation and design parameters

In this work, bio-inspired structures are modeled as Voronoi structures, where their ligaments form polygonal cells that fill the design domain. The Voronoi diagrams are generated using the Qhull algorithm [23], which forms polygonal cells by calculating boundaries around each seed point, ensuring that each cell represents the region closest to its corresponding seed point. As a result of the tessellation process, the configuration of the Voronoi diagram is influenced by the number and initial positions of the seeds. For example, more regular and smaller polygons form in regions where the seeds are densely populated and uniformly distributed.

To reflect and parameterize natural patterns in bio-inspired structures, it is necessary to select design variables that can control both the

uniformity and quantity of the initial seeds. In this work, the Simple Sequential Inhibition (SSI) process is adopted, as suggested by Martinez et al. [24], and which is widely utilized to replicate natural patterns [25,26,27,28] due to its simplicity and effectiveness. The approach sequentially generates and evaluates seeds, discarding those within a minimum threshold distance s from existing points.

$$s = \delta \times \sqrt{\frac{2A}{\sqrt{3}n}} \tag{1}$$

where s is the threshold distance between seeds, determined by the regularity δ and the number of seeds n under the design domain area A [29,30]. By controlling s through these two independent Voronoi parameters—the regularity and the number of seeds—the threshold distance can be adjusted to implicitly govern the final configuration of the Voronoi structure.

For simplicity, the ligament thickness t is assumed to be uniform, and it is calculated based on the total length of the ligaments l_i and the amount of material allocated for the structure $V_{volfrac}$:

$$V_{volfra} = \sum_{i=1}^{n} \frac{tl_i}{V_d} \tag{2}$$

Although the Voronoi tessellation is a highly efficient process, the SSI process requires considerable computational overhead as the regularity δ approaches unity (i.e., a uniform structure). According to probability theory, it is unlikely to create completely regular seeding for large numbers [31]. To address these challenges, some approaches involve leveraging a designer's intuition [32] or introducing perturbations to regular Voronoi structures [33]. In this study, the design space is reduced to ensure that the optimization iterations remain computationally feasible: $\delta \in [0, 0.7]$ and $n \in [2, 40]$.

Fig. 1 exemplifies the design of a Voronoi structure considered in the study. The cellular structure is designed within the square design domain, with the same height D_{sh} and width D_{sw}, which is padded by two plates located at the top and bottom. These plates are treated as rigid bodies to provide sufficient compression to the structure without experiencing any significant deformation themselves [34].

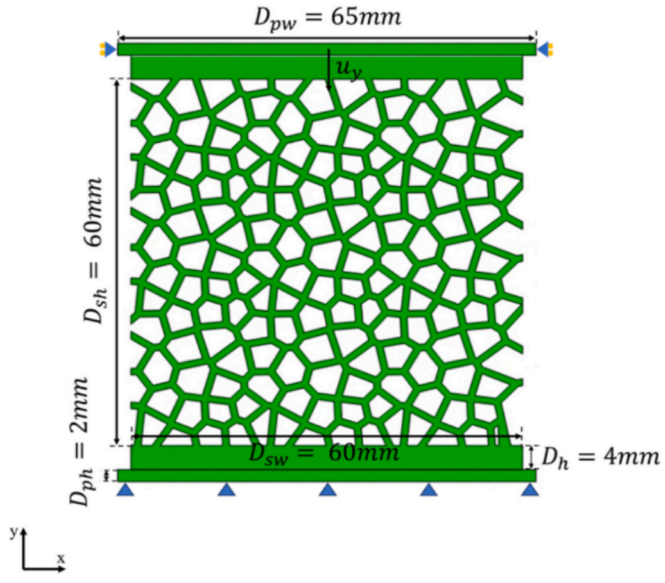

Fig. 1. Schematic illustration of the finite element method model and boundary conditions used for the uniaxial compression simulation.

2.2. FE analysis of an energy absorption phenomenon

In this study, bio-inspired structures are subjected to quasi-static in-plane compression loading, a widely used method for evaluating the EA capability in various engineering applications, including protective systems [34,35]. Fig. 2 illustrates the typical force–displacement curve during the uniaxial compression of bio-inspired foams. The EA capability of a structure in uniaxial compression is typically defined as the area under the force–displacement curve [36,37]. The curve is generally divided into three regions: elastic, plateau, and densification [38]. The structure first deforms elastically until it reaches the plateau region, where the ligaments buckle and the structure collapses. It is worth noting that the plateau region, where the force increase is suppressed due to cascading collapse and yielding, predominantly governs the EA capability of the structures. This region ends when the structure becomes fully densified, leading to a steep rise in force. In this study, the densification displacement is defined as the displacement at which the slope of the tangent equals that of the elastic regime [39], a commonly used approach in EA evaluations [40,41].

The force–displacement curve is obtained using high-fidelity nonlinear finite element analysis with the commercial software ABAQUS 2020, following [42,43], due to the substantial structural nonlinearities in compression, including self-contact and plastic deformation of the constituting ligaments. The contact properties were set with a friction coefficient of 0.3 for tangential behavior and hard contact for normal behavior to prevent penetration between ligaments. For simplicity, a plane strain condition is assumed, and 4-node plane strain elements (CPE4R) are used to model the structure. The simulation employed the elastoplastic properties of nylon, characterized by a Young's modulus of 305.41 MPa and a Poisson's ratio of 0.4. For the plastic regime, isotropic hardening was assumed, with the yield stress starting at 15.91 MPa and increasing up to 206.90 MPa at a plastic strain of 0.67 to accurately model the material behavior under compression, as detailed in [44]. Additionally, the compression plate was modeled as a rigid body to prevent deformation during loading, following [45]. The reaction force of the structure during uniaxial compression was extracted from the reference point, where the rigid body constraint was applied to the upper plate. The yield stress and plastic strain data used to evaluate the EA performance of the Voronoi structures are presented in Table A1. To validate the simulation setup, experimental verification was conducted using three representative models: the reference model from [44], a honeycomb structure, and a randomly selected Voronoi structure. The results showed that the errors in EA were approximately 9 %, 6.35 %, and 4 %, respectively, while the force–displacement curves exhibited good agreement with the experimental data, as shown in Fig. A1.

Given that this framework requires repeated evaluations of EA capabilities across multiple Voronoi configurations with varying Voronoi parameters (δ, n), it is crucial to establish a mesh resolution that ensures both accuracy and computational efficiency. To validate the reliability of the simulation results, a mesh convergence study was conducted as shown in Fig. B1. To assess the impact of mesh resolution, ten representative models were selected. Through the mesh convergence test, it was determined that setting the number of elements across the ligament thickness (n_t) to 4 provides an optimal balance between computational cost and model accuracy. Accordingly, all simulations in this study were conducted with $n_t = 4$. Further details on the mesh resolution analysis can be found in Appendix B.

2.2.1. EA variations for Voronoi random variables

As outlined in the preceding discussion, the generation of Voronoi structures is considered a random process for a given design variable, and the computation of their EA capability is regarded as realizations. Fig. 3 demonstrates five samples with ten function evaluations, where variances differ by up to 85 %. These differences arise from the Voronoi parameters that control the seed arrangement within the design domain.

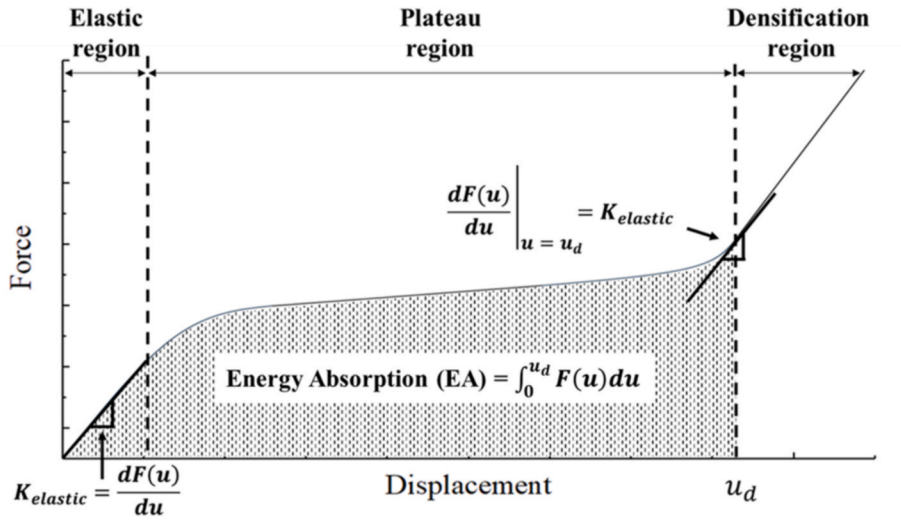

Fig. 2. Typical force-displacement curve of cellular structures under uniaxial compression, showing three regions: elastic, plateau, and densification [38].

Samples \ Case	1	2	3	4	5
1st	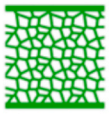 EA : 153.13	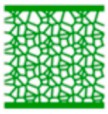 EA : 146.88	 EA : 135.04	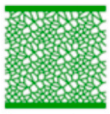 EA : 155.63	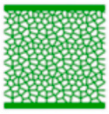 EA : 164.05
2nd	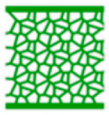 EA : 140.63	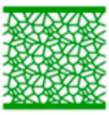 EA : 116.25	 EA : 131.25	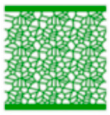 EA : 131.88	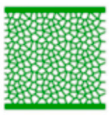 EA : 150.98
3rd	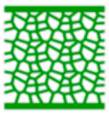 EA : 162.58	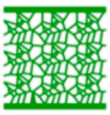 EA : 128.13	 EA : 115.68	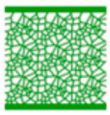 EA : 144.38	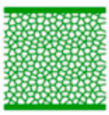 EA : 167.69
⋮	⋮	⋮	⋮	⋮	⋮
9th	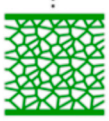 EA : 158.13	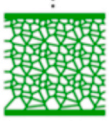 EA : 148.13	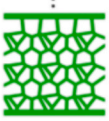 EA : 152.51	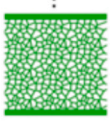 EA : 160.05	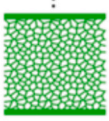 EA : 157.53
10th	 EA : 134.38	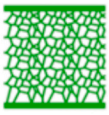 EA : 169.38	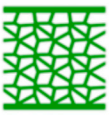 EA : 144.38	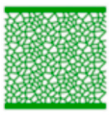 EA : 150.63	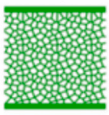 EA : 161.39
Design variable	δ : 0.4665 n : 10	δ : 0.0438 n :17	δ : 0.1412 n : 6	δ : 0.3792 n : 33	δ : 0.6581 n : 27
Variance in EA	120.0867	463.9327	371.0771	105.9932	51.59196

Fig. 3. Illustration of the five Voronoi parameters, where ten function evaluations were performed to assess the EA and quantify the aleatory uncertainty in Voronoi structures.

As regularity increases, the minimum distance between seeds also increases, leading to more uniform seed distributions. Consequently, the configurations of the Voronoi structures become more uniform, reducing variance in the EA capabilities. A greater number of seeds requires the minimum allowable distance between seeds—set by the regularity—to be maintained across all seeds, thereby minimizing

variance in EA performance.

3. Structural optimization maximizing EA

3.1. Problem statement

To design the optimal Voronoi structure, the optimization problem to maximize EA for the given amount of material is formulated as:

$$\underset{\delta,n}{argmax} \int F(u)du \quad \text{subject to } V(\delta,n) = V_{volfrac} \tag{3}$$

where δ and n are design variables characterizing the Voronoi diagram, $V_{volfrac}$ represents the volume fraction, and $\int F(u)du$ is the area under the force–displacement curve. Considering that n is an integer, a rounding-off process was applied before the generation of the Voronoi structures and surrogate modeling. The volume fraction was fixed at 0.38 to enable comparison of the EA of the optimal Voronoi structures with those presented in reference [44]. In the proposed design framework, a single objective function evaluation was performed for design variables selected by BO, integrating the force–displacement curve for each Voronoi structure defined by δ and n. Additionally, a reference BO is performed with 40 objective function evaluations per candidate BO selected in Section 4 to assess the metamodel accuracy and global optimum search capability of the proposed BO. The evaluations were averaged to construct the Kriging model for the reference BO, accounting for the aleatory uncertainty in the Voronoi structures. The reference BO is performed in the Results and discussion section for the metamodel accuracy and global optimum search capability of the proposed BO.

3.2. Design framework

In the present work, BO is employed to optimize the Voronoi parameters for superior EA performance, considering the complex and stochastic relationship between EA and design variables. BO is particularly well-suited for managing the complex and computationally intensive function evaluations, where the relationship between Voronoi parameters and EA capability of Voronoi structures is treated as a black box. Furthermore, BO addresses aleatory uncertainty in Voronoi structures by incorporating probabilistic information into the surrogate model. Specifically, Kriging is used as the surrogate model, with a nugget to account for the aleatory uncertainty, providing a practical alternative to approaches requiring extensive simulations like Monte Carlo methods. By relying on observed data, rather than requiring a deep understanding of physics in the system, BO lowers the barrier to the design process for Voronoi structures. A theoretical explanation of the methodologies used in the proposed design framework is provided in the following sections.

Fig. 4 illustrates the proposed design framework for Voronoi structures with superior EA capabilities, comprising three key steps: (1) initial sampling to quantify the aleatory uncertainty in the Voronoi structures, where 40 function evaluations are performed for each set of initial design variables, (2) the BO cycle to optimize the Voronoi random variables (e.g., δ and n) where aleatory uncertainty is incorporated into the surrogate model, enabling a single function evaluation per set of design variables selected by BO and significantly reducing the number of expensive function evaluations needed for optimizing EA—a strategy not previously explored in this context. (3) the generation of multiple solutions based on the optimal Voronoi parameters. It is worth noting that the variability in Voronoi configurations provides designers with a wide range of options when creating Voronoi structures.

3.2.1. Bayesian optimization

For BO, Kriging was selected as a probabilistic surrogate model, where the predicted response of a random variable $\mathbf{x}$ follows a multivariate Gaussian distribution $N\left(\hat{y}(\boldsymbol{x}), \hat{\sigma}(\boldsymbol{x})^2\right)$. Based on the assumption, the improvement of $\mathbf{x}$ beyond the best observed so far $y_{max} = \max\left(y(\boldsymbol{x}^{(1)}), \cdots, y(\boldsymbol{x}^{(n)})\right)$ can be defined [46] as

$$I(\boldsymbol{x}) = \max(\hat{y}(\boldsymbol{x}) - y_{max}, 0) \tag{4}$$

With the expectation of improvement, an infill strategy known as Expected Improvement (EI) can be derived in a closed-form expression. In this study, EI is utilized as the acquisition function for optimization [46]:

$$\mathbb{E}[I(\boldsymbol{x})] \begin{cases} (\hat{y}(\boldsymbol{x}) - y_{max})\Phi\left(\dfrac{\hat{y}(\boldsymbol{x}) - y_{max}}{\hat{\sigma}(\boldsymbol{x})}\right) + \hat{\sigma}(\boldsymbol{x})\phi\left(\dfrac{\hat{y}(\boldsymbol{x}) - y_{max}}{\hat{\sigma}(\boldsymbol{x})}\right) & \text{if } \hat{\sigma}(\boldsymbol{x}) > 0 \\ 0 & \text{else} \end{cases} \tag{5}$$

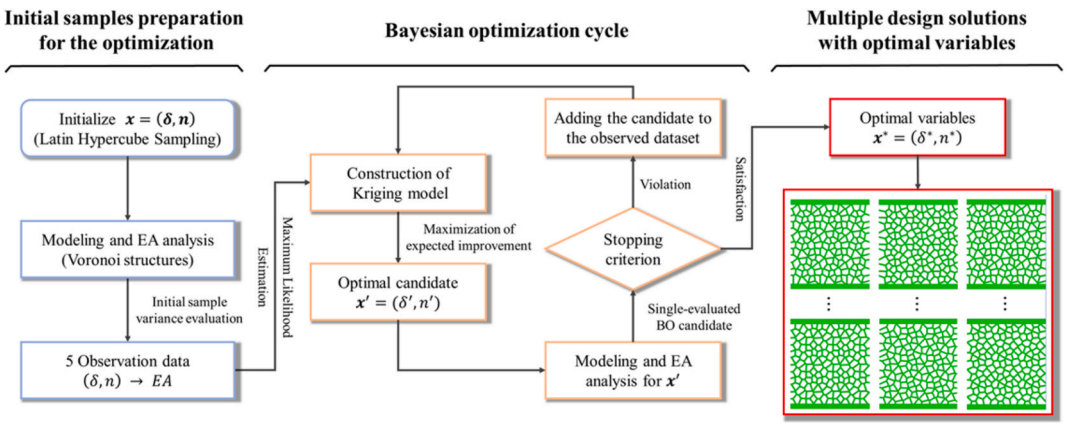

Fig. 4. Schematic diagram of the proposed Voronoi structure design framework for the superior EA capability, consisting of three steps: initial sample preparation and evaluation of Voronoi structures, BO cycle to optimize the Voronoi random variables (δ, n),and the generation of multiple solutions with respect to the optimal design variable.

where y_{max} represents the best objective value observed. The term $\widehat{y}(x)$ and $\widehat{\sigma}(x)$ denote the predicted mean and standard deviation by Kriging at $\boldsymbol{x}$, respectively. ϕ and Φ are the probability density function and the cumulative distribution function of the standard normal distribution.

This acquisition function employs an elegant trade-off by prioritizing candidates with both a high expected mean and variance, combining the two core strategies of exploration and exploitation, as characterized by the EI criterion. The exploitation strategy, represented by the first term in Eq. (5), aims to obtain design variables that show superior objective function values across the design domain. In contrast, the exploration strategy, indicated by the second term, focuses on design variables associated with high variance in the predicted response surface. The next design variable to be evaluated is suggested based on Eq. (6), which shows the highest EI value across the design domain. The iterative process is repeated until no improvement in the objective function is observed, even after more than five iterations.

$$\boldsymbol{x}^{(n+1)} = \underset{\boldsymbol{x}}{\operatorname{argmax}} EI(\boldsymbol{x}) \tag{6}$$

The selected design variable $\boldsymbol{x}^{(n+1)}$ is then evaluated and is used to update the probabilistic surrogate model [46].

3.2.2. Kriging

The Kriging surrogate model is constructed with a constant regression term, as follows [44]:

$$y(\boldsymbol{x}) = \boldsymbol{\alpha} + Z(\boldsymbol{x}) \tag{7}$$

where $y(\boldsymbol{x})$ is the predicted mean at the design variable $\boldsymbol{x}$, $\boldsymbol{\alpha}$ is the best linear unbiased predictor (BLUP), and Z($\boldsymbol{x}$) is the stochastic error function at design variable $\boldsymbol{x}$ following a Gaussian distribution with zero mean and the process variance σ_P^2. In this study, spatial correlation was assumed among the Voronoi random variables, and the Matérn 5/2 kernel was employed for the correlation matrix, which is commonly used to define the spatial relationship between design variables [48]. Additionally, the aleatory uncertainty of Voronoi random variables is incorporated as a nugget into the Matérn kernel to address the inherent variability of Voronoi structures, as shown in Eq. (8) [47].

$$\boldsymbol{R}(\boldsymbol{x}_\alpha, \boldsymbol{x}_\beta, \boldsymbol{\theta}) = \left(1 + \frac{\sqrt{5}\,|x_{\alpha i} - x_{\beta i}|}{\theta_i} + \frac{5}{3\theta_i^2}\right) exp\left(-\frac{\sqrt{5}\,|x_{\alpha i} - x_{\beta i}|}{\boldsymbol{\theta_i}}\right) + \lambda \mathrm{I} \tag{8}$$

where N is the dimension of design variables, $x_{\alpha i}$ and $x_{\beta i}$ are the i-th components of two observations $\boldsymbol{x}_\alpha$ and $\boldsymbol{x}_\beta$ respectively, θ_i is the coefficient of correlation, defining the extent of correlation among the i-th elements, λ is the nugget term representing intrinsic variance at each observation and I is the identity matrix.

This approach accounts for noisy observations, preventing overfitting and enhancing the robustness of predictions for unobserved data in a noisy dataset [49]. Specifically, when the Kriging model handles random variables showing high aleatory uncertainty with very close Euclidean distances or identical ones, the condition number of the correlation matrix becomes exceedingly high, leading to the failure of constructing the surrogate model [50]. As previously mentioned, a single function evaluation was conducted for each BO candidate and the aleatory uncertainty obtained from the initial samples was incorporated as a nugget term to prevent numerical instability. This approach reduced computational loads for the optimization while preserving the surrogate model's accuracy. It is worth noting that BO considering the nugget with single function evaluation prevents rank deficit of the Gram matrix and avoids failure in finding global optimum due to insufficient search over the design domain.

In this study, homoscedastic noise was utilized as a nugget, adopting the lowest variance observed among the initial samples throughout the entire optimization process. This approach was chosen because applying a large variance of initial samples to the correlation matrix would result in a surrogate model that is too smooth to optimize Voronoi variables for high EA [51].

Building upon the modified correlation matrix, the optimal hyperparameter $\boldsymbol{\theta}^*$ is obtained through Maximum Likelihood Estimation (MLE) using the quasi-Newton method, which maximizes the likelihood based on the observations. For a detailed derivation, please refer to references [52]. With $\boldsymbol{\theta}^*$ obtained, BLUP and process variance are expressed as follows [52]:

$$\begin{aligned} \boldsymbol{\alpha} &= \left(1^T \boldsymbol{R}^{-1} 1\right)^{-1} \left(1^T \boldsymbol{R}^{-1} \boldsymbol{Y}\right) \\ \sigma_p^2 &= \frac{1}{M} (\boldsymbol{Y} - \boldsymbol{\alpha} 1)^T \boldsymbol{R}^{-1} (\boldsymbol{Y} - \boldsymbol{\alpha} 1) \end{aligned} \tag{9}$$

where M represents the number of observations, **1** is a unit vector of dimension N, and **Y** is the response vector corresponding to each design variable. Utilizing the unbiased estimator and process variance, the expected mean and variance of the probabilistic surrogate model are then derived as follows [52]:

$$\begin{aligned} \widehat{\boldsymbol{y}}(\boldsymbol{x}) &= \boldsymbol{\alpha} + \boldsymbol{r}(\boldsymbol{x})^T \boldsymbol{R}^{-1} (\boldsymbol{Y} - \boldsymbol{\alpha} 1) \\ \widehat{\boldsymbol{\sigma}}^{\,2}(\boldsymbol{x}) &= \sigma_p^2 \left[1 + \boldsymbol{\mu}^T \left(1^T \boldsymbol{R}^{-1} 1\right)^{-1} \boldsymbol{\mu} - \boldsymbol{r}(\boldsymbol{x})^T \boldsymbol{R}^{-1} \boldsymbol{r}(\boldsymbol{x})\right] \end{aligned} \tag{10}$$

where $\mu = 1^T \boldsymbol{R}^{-1} \boldsymbol{r} - 1$ and the vector $\boldsymbol{r}(\boldsymbol{x})^T = [\boldsymbol{R}(\boldsymbol{x}, \boldsymbol{x}_1), \boldsymbol{R}(\boldsymbol{x}, \boldsymbol{x}_2), \cdots, \boldsymbol{R}(\boldsymbol{x}, \boldsymbol{x}_N)]$.

4. Results and discussion

4.1. Design optimization

In this section, the accuracy and computational efficiency of the proposed Voronoi structure design framework are evaluated through two independent optimization trials with different initial samples, while simultaneously examining the influence of initial samples on the proposed framework and assessing its capability to achieve the global optimum. Fig. 5(a) and (b) depict the optimization histories where the EA of the Voronoi structure is maximized through BO, while Fig. 5(c) and 5 (d) show the force–displacement curves derived from the Voronoi parameters demonstrating improvements in the objective function during the optimization.

As shown in Fig. 5(a) and (b), both trials yield the same optimal solution $(\delta^*, n^*) = (0.7, 18)$ identified in the reference BO. The optimized designs exhibit improved average EA performance, with increases of 15.74 % and 11.20 % in the first and second trials, respectively. These improvements are measured against the initial sample set averages, where the highest observed EA values were 161.88 kJ and 165 kJ. It is worth noting that the difference in the converged EA value between trials arises because each EA value represents a single evaluation, rather than an averaged result as in the reference BO, which requires 40 function evaluations.

In addition, the proposed BO reduced the computational burden of function evaluations by up to 95.25 % compared to the reference BO, which required fewer iterations for optimization but a higher number of function evaluations per iteration. For example, the first optimization required 400 function evaluations in the reference BO, whereas the proposed method only needed 19 function calls. These findings demonstrate that the proposed method is superior in efficiency, with significantly reduced computational loads, while identifying global optima from which Voronoi structures exhibit superior EA performance.

It is worth noting that all iterative searches identify the same design variable of (δ^*, n^*), where the design layouts exhibit the highest regularity and a moderate number of seeds within the potential design space, as illustrated in Fig. 5 (c) and (d). It can be explained by the fact that EA improves as regularity increases. Greater regularity enhances resistance to compression, resulting in structures with higher stiffness in the elastic

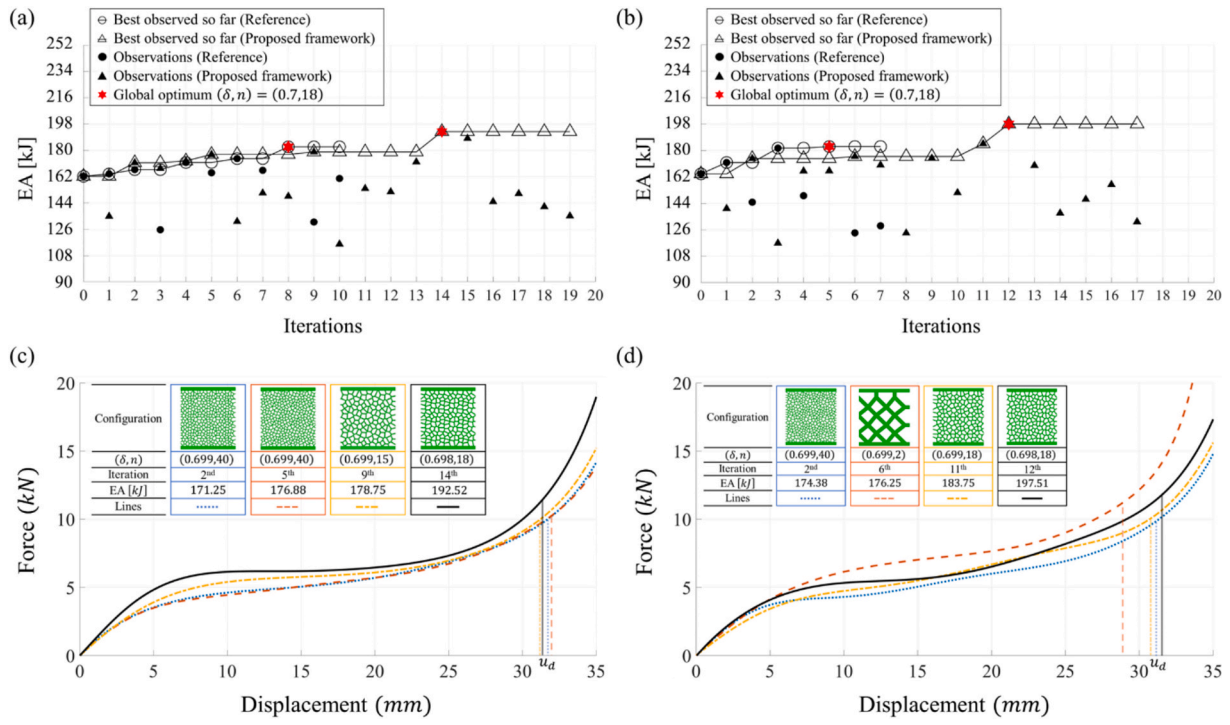

Fig. 5. Overview of the BO histories for designing Voronoi structures with superior EA capability: (a) and (b) show the proposed BO using triangles for predictions of the proposed metamodel and the reference BO using circles. Iteration zero represents the best average EA value among initial samples. (c) and (d) depict the force–displacement curves for the proposed BO candidates showing improvement during both optimizations along with the densification displacement, denoted by u_d.

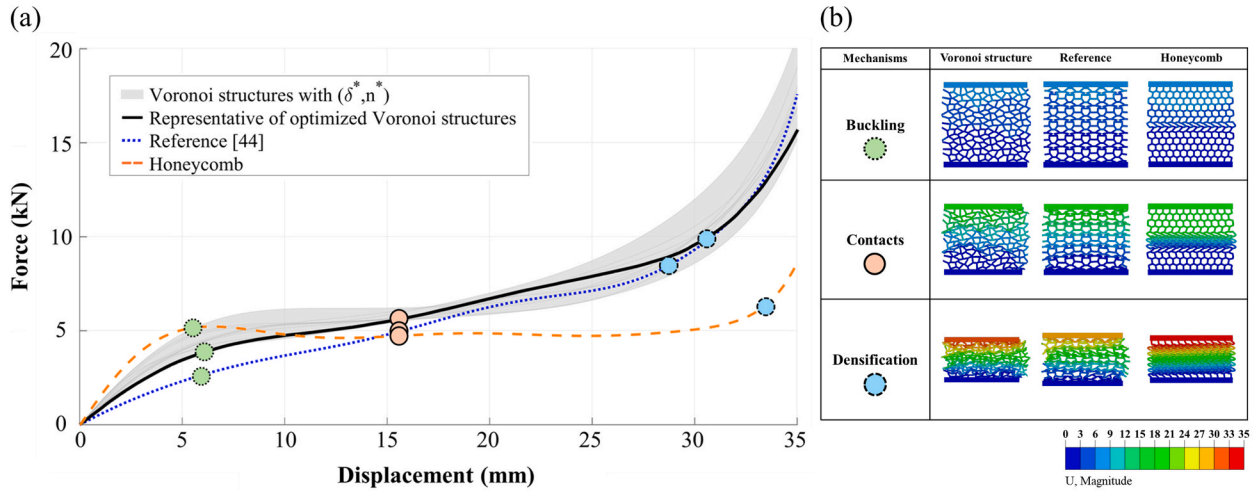

Fig. 6. (a) Force-displacement curves from uniaxial compression simulations comparing the optimized Voronoi structures, the reference model by Ghazlan et al. [44], and the honeycomb structure. (b) Three representative deformation mechanisms observed during compression—buckling (green circle with a dashed outline), contact (red circle with a solid outline), and densification (blue circle with a dashed outline)—are marked in (a) with corresponding color-coded indicators.

regime. Furthermore, a trade-off is observed as the number of seeds increases. Since the material volume remains fixed throughout the design search, configurations with higher n result in thinner ligaments, which exhibit greater densification displacement but lower stiffness.

The Voronoi structures generated for the same optimum, i.e., (δ^*, n^*), are further analyzed, as shown in Fig. 6. By sampling multiple optimal Voronoi structures, the average EA was found to be 181.93 kJ, with a minimum EA of 173.25 kJ among the samples. Notably, even the lowest EA performance of the optimal Voronoi structure exceeds the maximum EA of the initial samples at 169.81 kJ, showing that the proposed design method is capable of conceiving structures for superior EA.

Additionally, the results were compared with the bio-inspired model proposed by Ghazlan et al. (2020) [44], where the amount of material same as the optimized Voronoi structure was used, and demonstrated superior EA capability compared to well-known metamaterials. The optimized Voronoi structure exhibited up to 33.59 % higher EA than the reference model. To better understand the increase in EA capability, the deformation mechanisms of the Voronoi structures during uniaxial compression were identified, as shown in the inset. For comparison, one sample with an EA of 183.12 kJ was selected for illustration. The reference model exhibits minimal buckling of ligaments until the onset of densification, resulting in a hardening effect in the plateau region, but

also shows low initial stiffness and a small densification displacement (e.g., $u_d = 28.83$ mm). In contrast, the optimal Voronoi structures exhibit higher initial stiffness, a hardening effect in the plateau region, and a greater densification displacement (e.g.,$u_d = 31.87$ mm). This deformation mechanism is attributed to the randomized buckling throughout the structure, which prevents huge energy dissipation from buckling as the ligaments compact against each other during compression. The specific mechanisms behind these behaviors are further discussed in Section 4.3.

4.2. Accuracy of metamodel

The suggested framework assumes homoscedastic noise and evaluates each BO-selected candidate only once to update the surrogate model. This approach can introduce errors in the predicted EA response surface, potentially impeding the search for the global optimum in the design space. Therefore, a comparison was made between the Kriging models constructed in the proposed framework and the reference through two independent optimizations with different initial samples.

4.2.1. Effect of a nugget in optimization

As shown in Fig. 7, the global minimum for the Voronoi parameters is identified as $(\delta^*, n^*) = (0.7, 18)$. Two independent optimization runs starting from different initial samples consistently converge to the same global optimum, confirming the robustness of the proposed approach. In addition, the surrogate model constructed during the proposed BO demonstrates errors below 2 % in the vicinity of the global optimum (δ^*, n^*) by the end of the optimization, indicating that the proposed method successfully recreates an accurate surrogate model around (δ^*, n^*).

The high accuracy around the global optimum, despite the reduced number of function evaluations, can be attributed to the nugget term in Eq. (8), which accounts for the intrinsic variance approximated by the

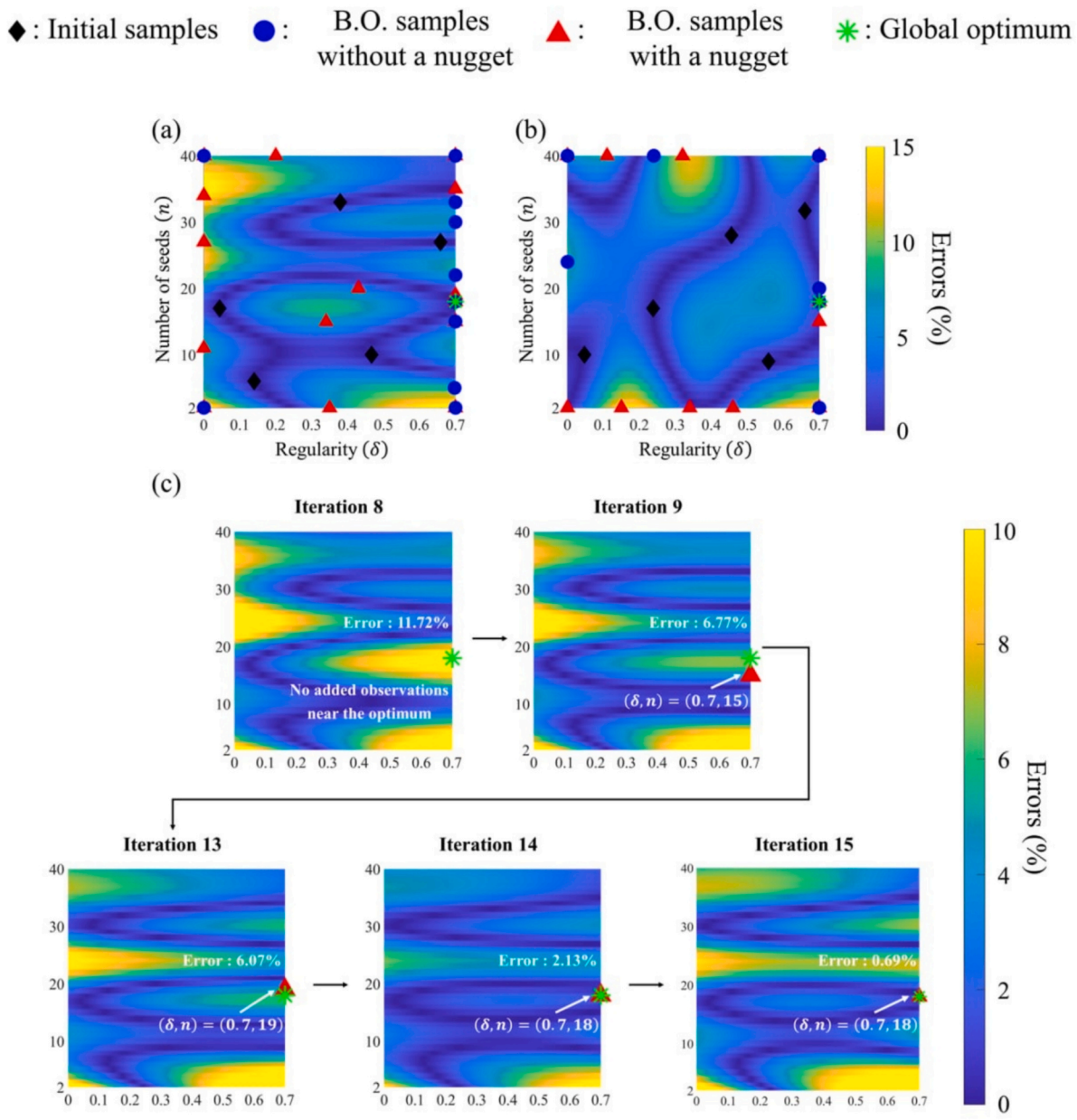

Fig. 7. Errors between the EA response surface with respect to Voronoi parameters for the proposed BO and the reference BO in two independent optimization processes: first (a) and second optimization (b), with the global optimum identified as $(\delta^*, n^*) = (0.7, 18)$. (c) illustrates the efficiency of the proposed design framework by iteratively sampling around the global optimum.

initial observations. It facilitates iterative sampling near the global optimum during the BO process, allowing for updates to the surrogate model and preventing rank deficiency and premature termination of the search. This process is highlighted in Fig. 7(c), where the proposed BO selected four candidates near the global optimum. Each observation is separately utilized to update the response surface, enhancing the accuracy of the predicted EA as more function evaluations are conducted near the global optimum.

It is worth noting that the errors are found in regions far from the global minimum due to the reduced number of samples in constructing the surrogate model. These errors can be attributed to the fact that the proposed BO relies on a single function evaluation that is insufficiently in capturing the statistical moments of the random Voronoi parameters at points such as $(\delta, n) = (0.7, 2)$ in Fig. 7(b). This, in addition to the effect of dissimilar initial sample sets, leads to wide variance in search paths between the proposed BO and the reference BO as observed at $(\delta, n) = (0, 35)$ in Fig. 7(a).

However, these discrepancies have a minimal impact on the optimization outcome as discussed in Section 4.1. The metamodel maintains over 98 % accuracy in predicting the EA capability of Voronoi structures near the global optimum, ensuring reliable optimization performance. Furthermore, both independent optimization trials successfully identify the optimal design variables regardless of the initial sample set, demonstrating the robustness of the proposed method. This trade-off between computational efficiency and accuracy—where errors in regions distant from the global optimum are tolerated to enhance optimization efficiency—remains acceptable within the scope of this study.

4.3. Mechanism of the improved EA

Fig. 6 shows the mechanical behavior of the three representative foams considered in the present study: a representative sample of the optimized Voronoi structures, a honeycomb structure, and the reference model suggested by Ghazlan et al. [44]. The figure presents the force–displacement relationship and can be distinguished into elastic, plateau, and densification regions following Fig. 2. Each deformation mechanism is illustrated in Fig. 6 (b).

In the elastic region, all three representative models exhibit a linear force–displacement relationship, effectively sustaining the applied load. Among them, the honeycomb structure demonstrates the highest stiffness, as previously reported in [44]. As deformation progresses into the plateau region, the primary deformation mechanism is characterized by buckling of ligaments. For the honeycomb structure, localized buckling occurs, leading to a cascading collapse that inhibits ligament interactions and results in a sudden drop in the curve as illustrated in Fig. 6 (a). Conversely, in the reference model, buckling occurs throughout the entire structure, inducing a hardening effect in the plateau region. The optimized Voronoi structure also displays a similar hardening effect, although the underlying mechanism differs; the buckling occurs at random locations, reflecting the distinctive deformation behavior shown in Fig. 6(b). The mechanism promotes ligament interactions, forming localized load-bearing regions that gradually enhance the stiffness of the Voronoi structure. With further deformation, the structure enters the densification region, where ligament compaction leads to a steep rise in the force–displacement curve.

The superior energy absorption capability of the Voronoi structure can be attributed to its optimized balance between stiffness and densification displacement, along with the presence of a hardening effect. A more detailed discussion of the relationship between these properties and the Voronoi parameters is provided later in this section. Compared to the honeycomb structure, the Voronoi structure exhibits relatively lower stiffness and densification displacement. Thanks to the fact that buckling occurs in a random manner, however, the gradual increase in the force–displacement curve within the plateau region allows for greater energy absorption than the honeycomb structure. Similarly, the reference model also exhibits a gradual increase in the curve within the plateau region. However, the optimized Voronoi structure achieves superior EA thanks to its higher stiffness and densification displacement compared to the reference model.

Building on the understanding of EA mechanisms in the optimized Voronoi structure, further analysis is conducted to examine how Voronoi parameters influence two key mechanisms—buckling and ligament densification—using five representative configurations that exhibit distinct variations in these behaviors, as shown in Fig. 8.

The first mechanism involves the buckling of individual ligaments, which is observed when the applied force exceeds the critical load of the structure. This buckling contributes to energy dissipation, thereby reducing the EA capacity of the structure. To quantify the resistance to buckling, the first critical force obtained by the eigenvalue buckling analysis is used.

The first mechanism is primarily related to the regularity parameter, which determines the aspect ratio of the polygons. For example, a structure (i.e., the first sample) with parameters $(\delta, n) = (0,\ 18)$ exhibits a substantially lower EA value compared to the optimal Voronoi struc-

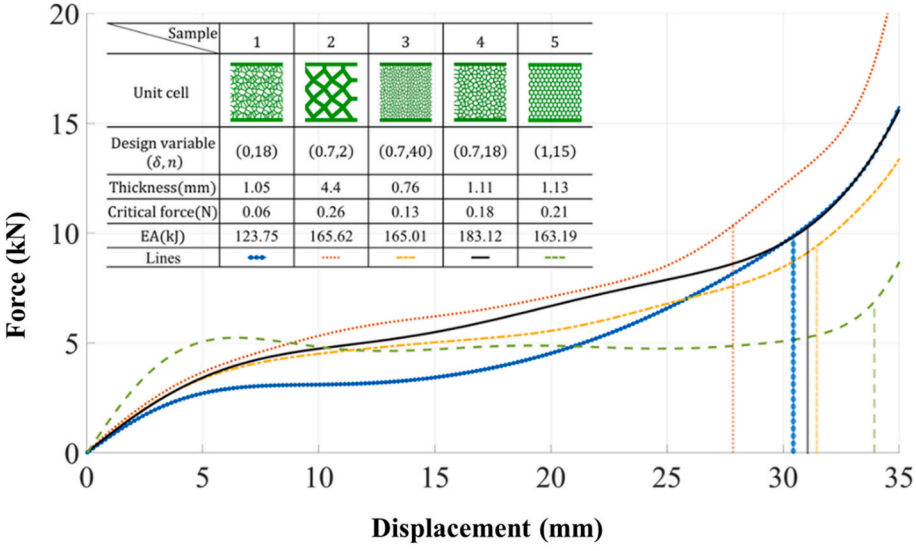

Fig. 8. Force-displacement curves under uniaxial compression simulation for Voronoi structures with varying Voronoi parameters, demonstrating the corresponding mechanical properties, such as ligament thickness, critical forces, and EA. The densification displacements are marked by vertical lines in the plots.

ture, despite having the same number of polygons within the design domain. This is because a decrease in regularity results in non-uniform polygons, which have diminished resistance to buckling under compression, thereby increasing energy dissipation. In contrast, a honeycomb structure with a regularity of 1 (i.e., the fifth sample) also shows a lower EA value than the optimal design, despite having a higher critical force. This phenomenon stems from cascading collapse in the structure, where insufficient interactions between ligaments reduce the EA capacity as illustrated earlier.

The second mechanism is ligament densification, which occurs as ligaments come into contact with each other, enhancing EA through increased densification displacement. The degree of ligament densification varies with the number of seeds, creating a trade-off between critical force and densification displacement. For instance, a structure with parameters $(\delta, n) = (0.7,\ 2)$ has the thickest ligaments but exhibits lower EA compared to the optimal design with (δ^*, n^*). This is because, despite having the highest critical load due to the thicker ligaments, the limited number of cells leads to reduced interaction between ligaments, causing the lowest densification displacement among the samples. Conversely, in the case of $(\delta, n) = (0.7, 40)$, although the structure shows the highest densification displacement due to the extensive ligament interaction, its EA capability is still lower than that of the optimal Voronoi structure. This is due to its lower resistance to compression from the thinner ligaments. This observation indicates that careful adjustment of the number of seeds is crucial to balancing resistance to buckling and ligament densification.

It is worth noting that the deformation mechanism during the crushing process of the foam is primarily governed by geometric nonlinearity. As a result, it is influenced by changes in the ligament network due to variations in the Voronoi parameters but is less affected by the stiffness of materials.

5. Conclusion

In this work, we introduce a novel BO-based design framework that efficiently optimizes Voronoi structures for superior EA capabilities using Voronoi parameters, which enable a stochastic yet efficient representation of the design space. To account for the aleatory uncertainty of Voronoi parameters, homoscedastic noise is introduced as a nugget term in the metamodeling process, ensuring numerical stability. The resulting metamodels demonstrate high accuracy near the global optimum, even with a reduced number of sample evaluations. Through this framework, the optimal Voronoi parameters $(\delta, n) = (0.7, 18)$ yield a range of structural configurations due to their stochastic nature. Nevertheless, all designs based on these parameters consistently exhibit excellent EA performance, characterized by high initial stiffness, hardening behavior in the plateau region, and decent densification displacement.

The proposed design framework can be applied to various domains beyond Voronoi structure design for EA capabilities. For instance, it can be extended to functionally graded foams with segmented Voronoi designs and other structural properties, offering superior tunability. Additionally, the framework can be used in experiments or other black-box simulations, broadening its range of applications. Moreover, the suggested approach enables the generation of structurally diverse configurations with superior mechanical properties using the same optimal design variable, efficiently expanding datasets required for generative design.

Nevertheless, this study has certain limitations. First, the suggested design framework has only been applied to EA maximization examples under uniaxial compression, while the framework has the potential to be applied to various EA applications, such as customized shoe midsoles. Second, the proposed framework considers a reduced design space, including a restricted range of the regularity parameter and the assumption of constant thickness, since the primary objective of this work is to propose an efficient design method that accounts for the stochastic characteristics of the structure while considering its complex mechanical behavior.

Although the present work is limited to geometric variations of foams and the resulting changes in their crushing mechanisms, the proposed gradient-free optimization framework is not limited to the fixed material. In future work, this approach will be extended to foams with material property variations that influence material nonlinearity, such as multi-material structures, functionally graded materials (FGMs), and plasticity.

CRediT authorship contribution statement

Youngtaek Oh: Writing – original draft, Software, Investigation, Conceptualization. **Byungjo Kim:** Writing – review & editing, Investigation, Software. **Hayoung Chung:** Writing – review & editing, Investigation, Conceptualization, Funding acquisition.

Declaration of competing interest

The authors declare that they have no known competing financial interests or personal relationships that could have appeared to influence the work reported in this paper.

Acknowledgements

This research was supported by National R&D Program through the National Research Foundation of Korea (NRF), funded by Ministry of Science and ICT (NRF-2020R1C1C1005741). This work also was supported by the Korea Institute of Energy Technology Evaluation and Planning (KETEP) and the Ministry of Trade, Industry & Energy (MOTIE) of the Republic of Korea (No. RS-2023-00240918), as well as by the National Research Foundation of Korea (NRF) grant funded by the Korea government (MSIT) (No. RS-2023-00257666). Additionally, this work was supported by Samsung Electronics Co., Ltd (IO221007-02753-01).

Appendix A

Table A1
Plastic properties of toughed Nylon utilized to evaluate EA performance of Voronoi structures.

Yield stress(MPa)	Plastic strain	Yield stress	Plastic strain	Yield stress	Plastic strain	Yield stress	Plastic strain
15.91	0	59.69	0.295	101.9	0.534	152.4	0.643
18.17	0.001	61.29	0.31	104.1	0.541	155.2	0.644
20.82	0.003	62.98	0.325	106.2	0.548	157.6	0.647
22.78	0.008	64.64	0.339	108.4	0.555	160.3	0.649
24.98	0.015	66.39	0.353	110.6	0.561	162.8	0.651

(*continued on next page*)

Table A1 (*continued*)

Yield stress(MPa)	Plastic strain	Yield stress	Plastic strain	Yield stress	Plastic strain	Yield stress	Plastic strain
27.3	0.024	68.12	0.366	112.8	0.568	165.4	0.653
29.6	0.034	69.86	0.379	115.1	0.573	167.9	0.655
31.99	0.047	71.81	0.391	117.4	0.579	170.4	0.657
34.53	0.062	73.68	0.403	119.8	0.584	173.1	0.658
37.21	0.08	75.54	0.415	122.1	0.589	175.8	0.659
39.76	0.099	77.33	0.426	124.3	0.595	178.6	0.66
42.05	0.118	79.26	0.437	126.7	0.599	181.4	0.661
44.17	0.137	81.25	0.448	129	0.604	184	0.662
46.16	0.156	83.4	0.457	131.2	0.609	186.5	0.663
48.07	0.175	85.32	0.467	133.5	0.613	189	0.664
49.77	0.193	87.4	0.476	135.7	0.618	191.4	0.666
51.5	0.211	89.48	0.485	138.1	0.622	193.9	0.667
53.12	0.229	91.48	0.494	140.5	0.625	196.5	0.668
54.76	0.246	93.53	0.503	142.9	0.629	199.2	0.668
56.41	0.263	95.56	0.511	145.2	0.633	201.8	0.669
58.05	0.279	97.71	0.519	147.4	0.637	204.4	0.669
59.70	0.294	99.79	0.527	149.8	0.64	206.9	0.67

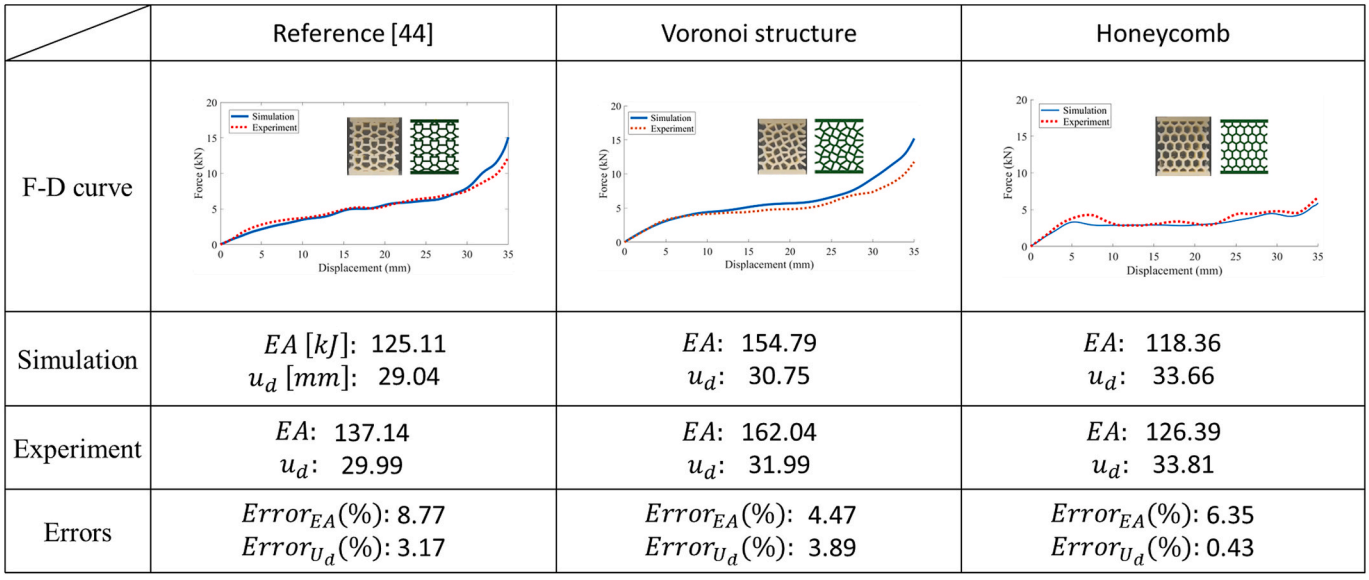

Fig. A1. Validation of numerical simulations through comparison with experimental compression data, where EA denotes the EA capability of a structure and represents densification displacement. and indicate the percentage differences between experimental and simulated values of EA and , respectively, relative to the experimental values.

Appendix B

As shown in Fig. B1, using more than 100,000 elements did not lead to noticeable differences in EA or densification displacement. Additionally, the force–displacement curves remained consistent, demonstrating that increasing the number of elements beyond this value had a negligible impact on the results. Based on this observation, this resolution was chosen as the reference for comparison. However, applying the reference resolution to all structural configurations was computationally prohibitive.

To address this, the number of elements was varied for each configuration, as shown in sample 1 of Fig. B1. For clarity in visualization, sample 1 included force–displacement curves for various mesh resolutions, while the remaining cases only presented the reference resolution and the four-element resolution along the ligament thickness. The study indicates that assigning four elements along the ligament thickness was sufficient to replicate the results obtained with the reference resolution while maintaining accuracy. Specifically, the maximum error observed was 2.7047% in EA and 1.8538% in densification displacement. While these errors represent a slight trade-off in accuracy, they are considered acceptable given the significant increase in computational efficiency. Additionally, the force–displacement responses, as shown in Fig. B1, were highly consistent across different configurations, showing that this resolution effectively captures ligament buckling and hardening behavior in the plateau region while ensuring computational efficiency.

Based on these findings, in the proposed optimization process, n_t was set to ensure that at least four elements were assigned for EA evaluations.

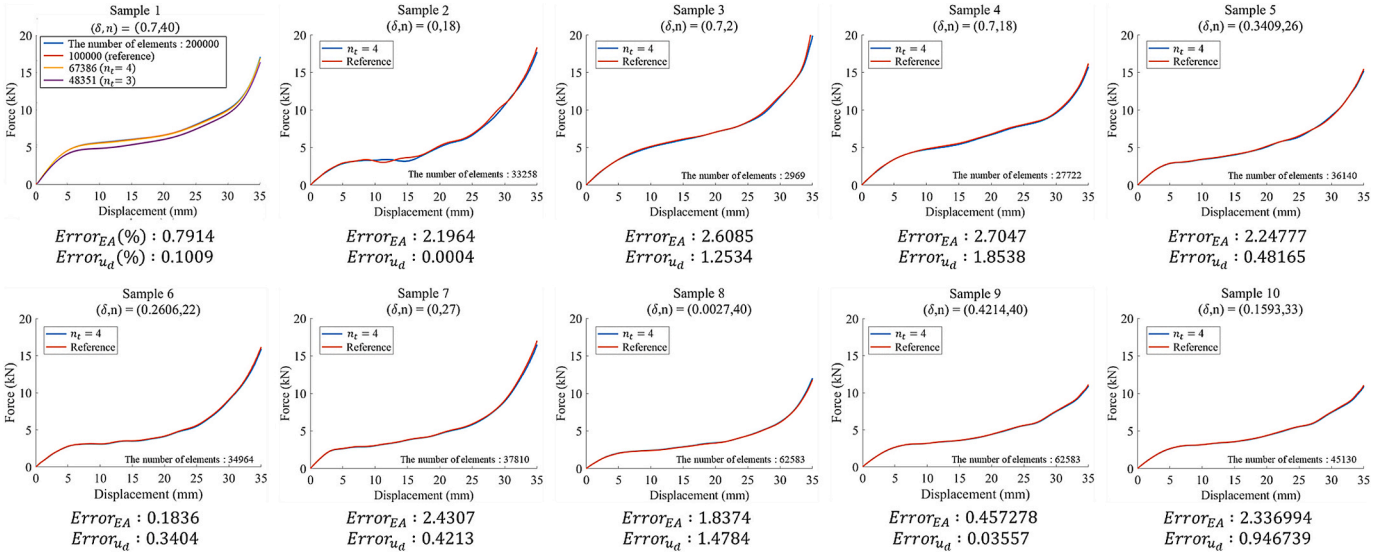

Fig. B1. Force-displacement curves of the Voronoi structure for ten representative samples, analyzed to examine mesh convergence and its effect on the accurate evaluation of EA capabilities. denotes the number of elements across the ligament thickness.

Data availability

Data will be made available on request.

References

[1] S.F. Fischer, M. Thielen, R.R. Loprang, R. Seidel, C. Fleck, T. Speck, A. Bührig-Polaczek, Pummelos as concept generators for biomimetically inspired low weight structures with excellent damping properties, Adv. Eng. Mater. 12 (12) (2010) B658–B663, https://doi.org/10.1002/adem.201080065.

[2] R. Seidel, M. Thielen, C. Schmitt, A. Bührig-Polaczek, C. Fleck, T. Speck, Fruit walls and nut shells as an inspiration for the design of bio-inspired impact resistant hierarchically structured materials, Design and Nature V (2010).

[3] Ngoc San Ha, Lu Guoxing, Dong Wei Shu, Yu Tx, Mechanical properties and energy absorption characteristics of tropical fruit durian (durio zibethinus), J. Mech. Behav. Biomed. Mater. 104 (2020) 103603, https://doi.org/10.1016/j.jmbbm.2019.103603.

[4] A. Bührig-Polaczek, C. Fleck, T. Speck, P. Schüler, S.F. Fischer, M. Caliaro, M. Thielen, Biomimetic cellular metalsusing hierarchical structuring for energy absorption, Bioinspiration & Biomimetics 11 (4) (2016) 045002, https://doi.org/10.1088/1748-3190/11/4/045002.

[5] W. Zhang, Sha Yin, Yu Tx, Xu Jun, Crushing resistance and energy absorption of pomelo peel inspired hierarchical honeycomb, Int. J. Impact Eng. 125 (2019) 163–172, https://doi.org/10.1016/j.ijimpeng.2018.11.014.

[6] Y. Nian, S. Wan, M. Avcar, R. Yue, M. Li, 3d printing functionally graded metamaterial structure: design, fabrication, reinforcement, optimization, Int. J. Mech. Sci. 258 (2023) 108580, https://doi.org/10.1016/j.ijmecsci.2023.108580.

[7] Y. Nian, S. Wan, M. Avcar, X. Wang, R. Hong, R. Yue, M. Li, Nature-inspired 3d printing-based double-graded aerospace negative poisons ratio metastructure: design, fabrication, investigation, optimization, Compos. Struct. 348 (2024) 118482, https://doi.org/10.1016/j.compstruct.2024.118482.

[8] Y. Nian, S. Wan, X. Wang, P. Zhou, M. Avcar, M. Li, Study on crashworthiness of nature-inspired functionally graded lattice metamaterials for bridge pier protection against ship collision, Eng. Struct. 277 (2023) 115404, https://doi.org/10.1016/j.engstruct.2022.115404.

[9] Z.e. Zhao, J. Li, D. Yao, Y. Wei, Mechanical and permeability properties of porous scaffolds developed by a Voronoi tessellation for bone tissue engineering, J. Mater. Chem. B 10 (2022) 9699–9712, https://doi.org/10.1039/D2TB01478E.

[10] H. Cheng, B. Liu, M. Liu, W. Cao, Design of three-dimensional voronoi strut midsoles driven by plantar pressure distribution, J. Comput. Des. Eng. 9 (4) (2022) 1410–1429, https://doi.org/10.1093/jcde/qwac060.

[11] A. Ghazlan, T.D. Ngo, P. Tran, Three-dimensional voronoi model of a nacre-mimetic composite structure under impulsive loading, Compos. Struct. 153 (2016) 278–296, https://doi.org/10.1016/j.compstruct.2016.06.020.

[12] Tee Y. Lu, T. Maconachie, P. Pille, M. Leary, T. Do, P. Tran, From nature to additive manufacturing: biomimicry of porcupine quill, Mater. Des. 210 (2021) 110041, https://doi.org/10.1016/j.matdes.2021.110041.

[13] J. Ortiz, G. Zhang, D.A. McAdams, A model for the design of a pomelo peel bioinspired foam, J. Mech. Des. 140 (11) (2018) 114501, https://doi.org/10.1115/1.4040911.

[14] Y. Song, Z. Wang, L. Zhao, J. Luo, Dynamic crushing behavior of 3d closed-cell foams based on voronoi random model, Mater. Des. 31 (9) (2010) 4281–4289, https://doi.org/10.1016/j.matdes.2010.04.007.

[15] Hamza Sulayman Abdullahi, Shuming Gao, A novel multi-cell square tubal structure based on voronoi tessellation for enhanced crashworthiness, Thin-Walled Struct. 150 (2020) 106690, https://doi.org/10.1016/j.tws.2020.106690.

[16] C.-C. Tung, Y.-Y. Lai, Y.-Z. Chen, C.-C. Lin, P.-Y. Chen, Optimization of mechanical properties of bio-inspired Voronoi structures by genetic algorithm, J. Mater. Res. Technol. 26 (2023) 3813–3829, https://doi.org/10.1016/j.jmrt.2023.08.210.

[17] Da. Chen, S. Kitipornchai, J. Yang, Dynamic response and energy absorption of functionally graded porous structures, Mater. Des. 140 (2018) 473–487, https://doi.org/10.1016/j.matdes.2017.12.019.

[18] Peter I Frazier. A tutorial on bayesian optimization. arXiv preprint arXiv 2018; 1807.02811. https://doi.org/10.48550/arXiv.1807.02811.

[19] B. Shahriari, K. Swersky, Z. Wang, R.P. Adams, N. De Freitas, Taking the human out of the loop: a review of Bayesian optimization, Proc. IEEE 104 (1) (2015) 148–175, https://doi.org/10.1109/JPROC.2015.2494218.

[20] D. Shin, A. Cupertino, M.HJ. de Jong, P.G. Steeneken, M.A. Bessa, R.A. Norte, Spiderweb nanomechanical resonators via bayesian optimization: inspired by nature and guided by machine learning, Adv. Mater. 34 (3) (2022) 2106248, https://doi.org/10.1002/adma.202106248.

[21] B. Kaczmarski, D.E. Moulton, A. Goriely, E. Kuhl, Bayesian design optimization of biomimetic soft actuators, Comput. Methods Appl. Mech. Eng. 408 (2023) 115939, https://doi.org/10.1016/j.cma.2023.115939.

[22] K. Park, Y. Kim, M. Kim, C. Song, J. Park, S. Ryu, Designing staggered platelet composite structure with gaussian process regression based bayesian optimization, Compos. Sci. Technol. 220 (2022) 109254, https://doi.org/10.1016/j.compscitech.2021.109254.

[23] C. Bradford Barber, D.P. Dobkin, H. Huhdanpaa, The quickhull algorithm for convex hulls, ACM Transactions on Mathematical Software (TOMS) 22 (4) (1996) 469–483, https://doi.org/10.1145/235815.235821.

[24] W.L. Martinez, A.R. Martinez, Computational statistics handbook with MATLAB, ChApman and Hall/CRC, 2001.

[25] V. Shulmeister, M.W.D. Van der Burg, E. van der Giessen, R. Marissen, A numerical study of large deformations of low-density elastomeric open-cell foams, Mech. Mater. 30 (1998) 125–140, https://doi.org/10.1016/S0167-6636(98)00033-7.

[26] Y.X. Gan, C. Chen, Y.P. Shen, Three-dimensional modeling of the mechanical property of linearly elastic open cell foams, Int. J. Solids Struct. 42 (26) (2005) 6628–6642, https://doi.org/10.1016/j.ijsolstr.2005.03.002.

[27] W.-Y. Jang, A.M. Kraynik, S. Kyriakides, On the microstructure of open-cell foams and its effect on elastic properties, Int. J. Solids Struct. 45 (7–8) (2008) 1845–1875, https://doi.org/10.1016/j.ijsolstr.2007.10.008.

[28] S. Gaitanaros, S. Kyriakides, A.M. Kraynik, On the crushing of polydisperse foams, European Journal of Mechanics-A/solids 67 (2018) 243–253, https://doi.org/10.1016/j.euromechsol.2017.09.010.

[29] H.X. Zhu, J.R. Hobdell, A.H. Windle, Effects of cell irregularity on the elastic properties of open-cell foams, Acta Mater. 48 (20) (2000) 4893–4900, https://doi.org/10.1016/S1359-6454(00)00282-2.

[30] H.X. Zhu, J.R. Hobdell, A.H. Windle, Effects of cell irregularity on the elastic properties of 2d voronoi honeycombs, J. Mech. Phys. Solids 49 (4) (2001) 857–870, https://doi.org/10.1016/S0022-5096(00)00046-6.

[31] É. Borel, La mécanique statique et l'irréversibilité, J. Phys. Theor. Appl. 3 (1) (1913) 189–196, https://doi.org/10.1051/jphystap:019130030018900.

[32] O.E. Sotomayor, H.V. Tippur, Role of cell regularity and relative density on elasto-plastic compression response of random honeycombs generated using voronoi diagrams, Int. J. Solids Struct. 51 (21–22) (2014) 3776–3786, https://doi.org/10.1016/j.ijsolstr.2014.07.009.
[33] V. Lucarini, From symmetry breaking to poisson point process in 2d voronoi tessellations: the generic nature of hexagons, J. Stat. Phys. 130 (2008) 1047–1062, https://doi.org/10.1007/s10955-007-9475-x.
[34] F.N. Habib, P. Iovenitti, S.H. Masood, M. Nikzad, In-plane energy absorption evaluation of 3d printed polymeric honeycombs, Virtual and Physical Prototyping 12 (2) (2017) 117–131, https://doi.org/10.1080/17452759.2017.1291354.
[35] C.I. Hammetter, R.G. Rinaldi, F.W. Zok, Pyramidal lattice structures for high strength and energy absorption, J. Appl. Mech. 80 (4) (2013) 041015, https://doi.org/10.1115/1.4007865.
[36] M. Wang, J. Zhang, W. Wang, L. Gao, Compression behaviors of the bio-inspired hierarchical lattice structure with improved mechanical properties and energy absorption capacity, J. Mater. Res. Technol. 17 (2022) 2755–2771, https://doi.org/10.1016/j.jmrt.2022.02.046.
[37] S. Xie, J. Zhang, X. Liu, S. Zheng, Z. Liu, A reinforced energy-absorbing structure formed by combining multiple aluminum foam-filled open-hole tubes, Int. J. Mech. Sci. 224 (2022) 107319, https://doi.org/10.1016/j.ijmecsci.2022.107319.
[38] Q.M. Li, I. Magkiriadis, J.J. Harrigan, Compressive strain at the onset of densification of cellular solids, J. Cell. Plast. 42 (5) (2006) 371–392, https://doi.org/10.1177/0021955X06063519.
[39] K.C. Chan, L.S. Xie, Dependency of densification properties on cell topology of metal foams, Scr. Mater. 48 (8) (2003) 1147–1152, https://doi.org/10.1016/S1359-6462(02)00593-6.
[40] M. Mohsenizadeh, F. Gasbarri, M. Munther, A. Beheshti, K. Davami, Additively-manufactured lightweight metamaterials for energy absorption, Mater. Des. 139 (2018) 521–530, https://doi.org/10.1016/j.matdes.2017.11.037.
[41] S. Gohar, G. Hussain, M. Ilyas, A. Ali, Performance of 3d printed topologically optimized novel auxetic structures under compressive loading: experimental and fe analyses, J. Mater. Res. Technol. 15 (2021) 394–408, https://doi.org/10.1016/j.jmrt.2021.07.149.
[42] X. Xiang, D. Shao, T. Pang, T.T. Ngo, N.S. Ha, S. Zhang, Energy absorption of multilayer aluminum foam-filled structures under lateral compression loading, Mech. Adv. Mater. Struct. 31 (3) (2024) 659–675, https://doi.org/10.1080/15376494.2022.2118405.
[43] Z. Khodaverdlou, S.S. Basir, P.K. Mohseni, Numerical and experimental investigation of energy absorption capacity in slotted thin-walled square tube structures, J. Braz. Soc. Mech. Sci. Eng. 44 (8) (2022) 368, https://doi.org/10.1007/s40430-022-03677-7.
[44] A. Ghazlan, T. Nguyen, T. Ngo, S. Linforth, et al., Performance of a 3d printed cellular structure inspired by bone, Thin-Walled Struct. 151 (2020) 106713, https://doi.org/10.1016/j.tws.2020.106713.
[45] F. Wu, Y. Chen, S. Zhao, Y. Hong, Z. Zhang, S. Zheng, Mechanical properties and energy absorption of composite bio-inspired multi-cell tubes, Thin-Walled Struct. 184 (2023) 110451, https://doi.org/10.1016/j.tws.2022.110451.
[46] D.R. Jones, M. Schonlau, W.J. Welch, Efficient global optimization of expensive black-box functions, J. Glob. Optim. 13 (1998) 455–492, https://doi.org/10.1023/A:1008306431147.
[47] D.G. Krige, A statistical approach to some basic mine valuation problems on the witwatersrand, J. South Afr. Inst. Min. Metall. 52 (6) (1951) 119–139.
[48] J. Snoek, H. Larochelle, R.P. Adams, Practical Bayesian optimization of machine learning algorithms, Adv. Neural Inf. Process. Syst. 25 (2012), https://doi.org/10.48550/arXiv.1206.2944.
[49] J.-L. Akian, L. Bonnet, H. Owhadi, É. Savin, Learning best kernels from data in gaussian process regression. with application to aerodynamics, J. Comput. Phys. 470 (2022) 111595, https://doi.org/10.1016/j.jcp.2022.111595.
[50] Hossein Mohammadi, Rodolphe Le Riche, Nicolas Durrande, Eric Touboul, and Xavier Bay. An analytic comparison of regularization methods for gaussian processes. arXiv preprint arXiv 2016; 1602.00853. .
[51] R.B. Gramacy, H.KH. Lee, Cases for the nugget in modeling computer experiments, Stat. Comput. 22 (2012) 713–722, https://doi.org/10.1007/s11222-010-9224-x.
[52] W.J. Sacks, T.J. Welch, Mitchell, and hp wynn,design and analysis of computer experiments, Stat. Sci. 4 (4) (1989) 409–453, https://doi.org/10.1214/ss/1177012413.